Chinese Journal of Chemical Engineering 59 (2023) 210–221

Contents lists available at ScienceDirect

Chinese Journal of Chemical Engineering

journal homepage: www.elsevier.com/locate/CJChE

Full Length Article

Measurement and model of density, viscosity, and hydrogen sulfide solubility in ferric chloride/trioctylmethylammonium chloride ionic liquid

Zhonghao Li, Yuanyuan Yang, Huanong Cheng *, Yun Teng, Chao Li, Kangkang Li, Zhou Feng, Hongwei Jin, Xinshun Tan, Shiqing Zheng

College of Chemical Engineering, Qingdao University of Science and Technology, Qingdao 266042, China

ARTICLE INFO

Article history:
Received 1 August 2022
Received in revised form 3 November 2022
Accepted 6 November 2022
Available online 15 December 2022

Keywords:
Ionic liquids
Hydrogen sulfide
Solubility
Henry's constant
Chemical reaction equilibrium constant
Model

ABSTRACT

The density and viscosity of ferric chloride/trioctylmethylammonium chloride ionic liquid (rFeCl$_3$/[A336]Cl) with different molar ratios (r = 0.1–0.8) of FeCl$_3$ to [A336]Cl were measured at temperatures from 313.15 to 358.15 K and atmospheric pressure. The density and viscosity data were fitted by the relevant temperature variation equations, respectively. The variation of density and viscosity with temperature and r was obtained. The solubility of rFeCl$_3$/[A336]Cl to H_2S was measured at temperatures from 318.15 to 348.15 K and pressures from 0 to 150 kPa. The effects of temperature, pressure, and r on the solubility of H_2S were discussed. The reaction equilibrium thermodynamic model (RETM) was used to fit the H_2S solubility data, and the average relative error was less than 1.3%, indicating that the model can relate the solubility data well. And Henry's constant and chemical reaction equilibrium constant were obtained by the RETM fitting. The relationships of Henry's constant and chemical reaction equilibrium constant with temperature and r were analyzed.

1. Introduction

Hydrogen sulfide (H_2S) is a colorless gas at room temperature with a special smell of rotten eggs. It is mainly produced in the processes of natural gas development, coal gasification, petroleum refining, ammonia production, sewage treatment, and paper manufacturing [1,2]. H_2S has flammable, explosive properties and strong toxicity [3]. H_2S in gaseous materials can cause serious corrosion of metal equipment and poisoning of the catalyst. H_2S in the atmosphere also causes acid rain, which is harmful to humans and the environment [4,5]. China has set strict standards for sulfur levels in environment and oil, which must not exceed 10 $\mu g \cdot g^{-1}$ [6,7]. Therefore, to control the environmental pollution caused by industrial production, gas desulfurization must be carried out.

The removal of H_2S by solvent absorption can be divided into physical absorption, chemical absorption, and wet oxidation. The physical absorption method (such as the Rectisol process [8]) has the advantage of low regeneration energy consumption. It is more suitable for high H_2S concentration. But it needs to be operated under high pressure and low temperature [9]. The most popular chemical absorption method is amine scrubbing [10], but it has some disadvantages such as foaming of aqueous solution and high regeneration energy consumption. Wet oxidation methods include ADA method [11], tannin extraction method [12], and complex iron method [13]. They have the advantages of high desulfurization efficiency, simple process, and operation at normal temperature and atmospheric pressure, so they have been widely in application [14]. However, there are still some problems with wet oxidation methods. For example, secondary salt (such as thiosulfate, sulfate, and sulfite) is produced during desulfurization [15]. To maintain the desulfurization efficiency, the waste liquid needs to be discharged from the absorption solution to keep the pH value of the solution stable between 9 and 10 [16].

Ionic liquids (ILs) are organic salt liquids at room temperature, composed of organic cations and inorganic or organic anions [17,18]. Ionic liquids have stable physical properties and low vapor pressure, which can hardly cause solution loss in the desorption process [19,20]. The structure of the ionic liquids are adjustable, which means researchers can design the ionic liquids according to the research object. Some metal ions (such as iron, aluminum, *etc.*) can be combined in the ionic liquids to form metal base ionic

* Corresponding author.
E-mail address: chn@qust.edu.cn (H. Cheng).

https://doi.org/10.1016/j.cjche.2022.11.012
1004-9541/

liquids. The iron-based ionic liquids (Fe-ILs) have oxidation and acidity [21]. H_2S is directly oxidized to elemental sulfur without the generation of secondary salt [22], which avoids the problem of waste liquid discharge of the existing wet oxidation methods.

He *et al.* [22] synthesized an imidazole-based Fe-IL named [Bmim]$Fe_{0.9}Cl_{4.7}$ using [Bmim]Cl and $FeCl_3{\cdot}6H_2O$. They found that the Fe-IL was hydrophobic and applied it to the removal of hydrogen sulfide gas. The desulfurization efficiency reached more than 99%. Guo *et al.* [23] used [Bmim]$FeCl_4$ ionic liquid to remove hydrogen sulfide gas. *N*,*N*-dimethylformamide was used as a solvent to improve the absorption performance.

Ma *et al.* [24] synthesized another kind of Fe-IL using Et_3NHCl and anhydrous $FeCl_3$, *r*$FeCl_3$/[Et_3NH]Cl (*r*, molar ratio of $FeCl_3$ to Et_3NHCl), and used it to remove H_2S in high-temperature gas. The results showed that 0.6$FeCl_3$/[Et_3NH]Cl had the best desulfurization efficiency, which was better than ordinary imidazole-based ionic liquid and Fe^{3+} aqueous solution. In addition, the sulfur generated in the reaction process was easier to separate. Li *et al.* [25] synthesized *r*$FeCl_3$/[Et_3NH]Cl with *r* from 0.56 to 0.71. They studied the influence of *r*, temperature, and pressure on the absorption of H_2S in ionic liquids. And they found that the maximal sulfur capacity of *r*$FeCl_3$/[Et_3NH]Cl was 2.178% (mass) at *r* of 0.67, the temperature of 303.15 K, and the pressure of 101.3 kPa.

In addition to the above two Fe-ILs ($FeCl_3$/[Bmim]Cl and $FeCl_3$/[Et_3NH]Cl), Kogelnig *et al.* [26] first synthesized ionic liquid [A336][$FeCl_4$]$_{0.73}$[Cl]$_{0.27}$ using [A336]Cl (methyl trioctyl ammonium chloride) and $FeCl_3{\cdot}6H_2O$. And magnetism and aggregation behavior of [A336][$FeCl_4$]$_{0.73}$[Cl]$_{0.27}$ were studied. Wang *et al.* [27] synthesized ionic liquid [A336]$FeCl_4$ using [A336]Cl and $FeCl_3{\cdot}6H_2O$. And [A336]$FeCl_4$ was combined with [Bmim]OH to absorb hydrogen sulfide at room temperature and atmospheric pressure. The results showed that [A336]$FeCl_4$ was stable, and sulfur content was up to 2.13%. The raw material for the synthesis of *r*$FeCl_3$/[A336]Cl ionic liquid is [A336]Cl. It is a quaternary ammonium salt that is widely used in the metal extraction [28,29] and has been industrially produced on a large scale. *r*$FeCl_3$/[A336]Cl has the advantage of low cost compared to expensive imidazole-based Fe-IL. Moreover, compared with $FeCl_3$/[Et_3NH]Cl, *r*$FeCl_3$/[A336]Cl has a larger molar volume, which means that the free space of the solution is larger and the solubility may be higher. Therefore, *r*$FeCl_3$/[A336]Cl has great application potential in the industrial application of H_2S removal from gas.

Density, viscosity, and solubility have important effects on the gas purification performance of Fe-ILs. Li *et al.* [30] measured density and viscosity of *r*$FeCl_3$/[Bmim]Cl (*r*, molar ratio of $FeCl_3$ to [Bmim]Cl) in the range of *r* from 1/1.7 to 1.5/1, *T* from 293.15 to 343.15 K. Density and viscosity decreased with the temperature increasing. Density increased with the *r* increasing, while viscosity decreased with the *r* increasing. As $1/1.7 \leq r \leq 1/1$, the viscosity decreased extremely, and the viscosity turned smoothly as $r \geq 1$. Cheng *et al.* [31] determined and modeled the solubility of hydrogen sulfide in *r*$FeCl_3$/[Bmim]Cl ionic liquid (*r*$FeCl_3$/[bmim]Cl, *r* = 0.6–1.4) at temperatures of 303.15 to 348.15 K and pressures of 100 to 1000 kPa. Henry's constant and chemical reaction equilibrium constant were obtained. To date, significant parameters of *r*$FeCl_3$/[A336]Cl, such as viscosity, density, and H_2S solubility, have not been reported. The actual oxidative desulfurization processes are operated at room temperature and atmospheric pressure. In this work, *r*[A336]$FeCl_4$ (*r*, molar ratio of $FeCl_3$ to [A336]Cl, *r* = 0.1, 0.2, 0.4, 0.6, and 0.8) ionic liquid was synthesized. Its density and viscosity were measured in the temperatures of 313.15 to 358.15 K under atmospheric pressure. Its solubility of H_2S was measured at temperatures of 318.15 to 348.15 K and pressures of 0 to 150 kPa. The experimental data of density, viscosity and H_2S solubility were fitted by models. The effects of temperature, pressure and molar ratio on density, viscosity and H_2S solubility were discussed.

2. Materials and Methods

2.1. Experimental reagents

H_2S gas was purchased from Yuyan Special Gas Co., Ltd. with a purity of 0.99. Anhydrous $FeCl_3$ was purchased from Aladdin Reagent Company with a purity of 0.995. [A336]Cl was provided from Macklin Reagent Company with a purity of 0.97. The pure water used in the density verification experiment was prepared by the UPR-II-5/10T equipment produced by Sichuan Youpu Ultra Pure Technology Co., Ltd.

r$FeCl_3$/[A336]Cl was synthesized according to the existing methods [26,27]. A certain amount of [A336]Cl was weighed into a beaker, and then slowly added anhydrous $FeCl_3$ with corresponding molar ratio while stirring. After full dissolution, the mixture was stirred continuously at 333.15 K for 24 h. Finally, the obtained *r*$FeCl_3$/[A336]Cl was transferred to a vacuum drying oven and dried at 333.15 K and 10 kPa for 48 h. *r*$FeCl_3$/[A336]Cl was further dried with 3A molecular sieve for several days before using. The water content was not detected due to the water content of *r*$FeCl_3$/[A336]Cl was below the detection limit (100 $\mu g{\cdot}g^{-1}$) of the Karl Fischer titrator (DL31, Mettler Toledo). The purity of *r*$FeCl_3$/[A336]Cl was determined by ultraviolet spectrophotometry (UV-1800, Shanghai Mepuda Instrument Co., Ltd.). Hydroxylamine hydrochloride was used to reduce ferric iron to ferrous iron. Divalent iron and ophenanthroline can form an orange-red complex, and the complex has a good absorbance at 512 nm of UV light. Before the measurement of Fe-IL, the ultraviolet spectrophotometer was calibrated with 100 $\mu g{\cdot}ml^{-1}$ standard-iron solution (Shanghai Aladdin Biochemical Technology Co., Ltd.). A sample description is presented in Table 1.

2.2. Density measurement

The density was measured by a Westphal balance (PZ-D-5, Shanghai Yueping Scientific Instrument Manufacturing Co., Ltd.). The measurement range was 0–2.0000 $g{\cdot}cm^{-3}$, and the uncertainty of the measured density was 0.0001 $g{\cdot}cm^{-3}$. The balance had a standard measuring hammer immersed in the liquid. Then various quantitative riding weights were putted in the V-shaped groove of the beam to maintain balance, and the specific gravity of the liquid was accurately measured. The calibration standard was that the specific gravity of pure water at 293.15 K was 1.0000. In this work, the temperature of the liquid was adjusted through a water recirculation bath (HH-Sc, Changzhou Langyue Co., Ltd.), and the temperature accuracy was ±0.03 K.

Table 1
Purities and sources of the samples used in the experiment

Chemical name	CAS number	Supplier	Purity
H_2S	7783-06-4	Yuyan Gas	0.99①
N_2	7727-37-9	Qingdao Hausen	0.9999①
$FeCl_3$	7705-08-0	Macklin	>0.995②
[A336]Cl	5137-55-3	Macklin	0.97②
r$FeCl_3$/[A336]Cl		This work	>0.98③
Glycerol	56-81-5	Macklin	99%②
Pure water	7732-18-5	Youpu ultrapure water machine (UPR-II-10 T)	Electrical resistivity > 18.2 MΩ·cm at 298 K

① The purity in mole fraction was provided by the supplier.
② The purity in the mass fraction was provided by the supplier.
③ The purity of the mass fraction of ionic liquid was measured by spectrophotometry.

2.3. Viscosity measurement

The viscosity was measured using a rotary digital viscometer (NDJ-4S, Shanghai Hengping Instrument Factory) with a measurement range of (1–2) × 10^6 mPa·s and measurement uncertainty of ±1%. Different rotors and rotational speeds were selected according to the predicted viscosity of the tested liquid. The viscosity of the liquid was calculated by measuring the viscosity moment of the liquid acting on the rotor at a constant speed. In this work, the temperature of the liquid was adjusted through a water recirculation bath (HH-Sc, Changzhou Langyue Co., Ltd.), and the temperature accuracy was ±0.03 K.

2.4. Solubility measurement

2.4.1. Experimental equipment and procedures

The experimental equipment for measuring the hydrogen sulfide solubility of rFeCl$_3$/[A336]Cl at temperatures of 318.15 to 348.15 K and pressures of 0 to 150 kPa is shown schematically in Fig. 1. The experimental equipment and procedures are similar to those reported in our previous work [31,32] for the measurement of H_2S solubility. The experimental equipment consists of a nitrogen gas cylinder, a hydrogen sulfide gas cylinder, a vacuum pump, a buffer tank, a phase equilibrium kettle (SL-Q100, Sen Long Equipment Company) with stirring, and a lye absorption bottle. The volume of the buffer tank is 547.4 ml, and the material is 316 stainless steel. The volume of the phase equilibrium kettle is 122.8 ml, and the material is Hastelloy alloy. The temperature of the buffer tank and the phase equilibrium kettle is adjusted through two constant temperature water baths with stirring (HH-Sc, Changzhou Langyue Co., Ltd.). The temperature is monitored by TES 1320 TYPE-K thermocouple, and the uncertainty is ±0.03 K. The pressure of the buffer tank and phase equilibrium kettle is monitored and transmitted to the computer by an integrated digital pressure gauge (YK-100B, Yunyi Instrument Co., ltd), and the uncertainty is 0.4 kPa.

A certain mass of ionic liquid ($w_{\text{Fe-IL}}$) was added to the equilibrium kettle with an uncertainty of ±3.0 × 10^{-8} kg. After checking the gas tightness of the experimental equipment, vacuumizing the system until the pressure was less than 0.1 kPa. At this stage, the system pressure was recorded as P_1. A certain amount of H_2S was filled into the phase equilibrium kettle through the buffer tank, and the pressure of the buffer tank before and after releasing H_2S was recorded as P_2 and P_3, respectively. Turned on the stirring device of the phase equilibrium kettle and started the absorption of H_2S. When the absorption in the phase equilibrium kettle reached equilibrium, the pressure of the phase equilibrium kettle was recorded as P_4. Finally, after the experiment had been completed, the residual H_2S in the system was discharged into the lye absorption flask.

2.4.2. Calculation of solubility

At gas–liquid equilibrium, the total solubility of H_2S in ionic liquid can be expressed by a molar fraction ($x_{t,i}$) and molality based on unit ionic liquid mass ($m_{t,i}$). They are given by Eq. (1) and Eq. (2).

$$x_{t,i} = \frac{n_{t,i}}{n_{t,i} + n_{\text{Fe-IL}}} \tag{1}$$

$$m_{t,i} = \frac{n_{t,i}}{w_{\text{Fe-IL}}} \tag{2}$$

where, $m_{t,i}$ is moles of H_2S per unit mass of ionic liquid. $n_{\text{Fe-IL}}$ and $w_{\text{Fe-IL}}$ are the moles and mass of the ionic liquid, respectively. $n_{t,i}$ is the moles of H_2S in the ionic liquid at the i-th absorption experiment. $n_{t,i}$ can be calculated from Eq. (3) and Eq. (4).

$$n_{t,i} = n_{t,i-1} + \Delta n_i \tag{3}$$

$$\Delta n_i = n_{a,i} - n_{g,i} + n_{g,i-1} \tag{4}$$

where, Δn_i is the incremental moles of H_2S absorbed in the ionic liquid in the i-th experiment. $n_{t,i-1}$ is moles of H_2S in the ionic liquid at the $(i-1)$-th experiment. When $i = 1$, $n_{t,i-1} = 0$. $n_{a,i}$ is moles of H_2S transferred from the buffer tank to the equilibrium kettle in the i-th experiment. $n_{g,i-1}$ and $n_{g,i}$ are moles of H_2S in the gas phase of the equilibrium kettle when gas and liquid phases reach equilibrium in the $(i-1)$-th and i-th experiment, respectively.

$n_{a,i}$ and $n_{g,i}$ are calculated from Eq. (5) and Eq. (6) of state for a real gas.

$$n_{a,i} = \frac{V_1}{RT}\left(\frac{P_{2\text{H}_2\text{S},i}}{Z_{2,i}} - \frac{P_{3\text{H}_2\text{S},i}}{Z_{3,i}}\right) \tag{5}$$

$$n_{g,i} = \frac{P_{\text{H}_2\text{S},i}(V_2 - V_L)}{Z_{\text{H}_2\text{S},i}RT} \tag{6}$$

where T is the equilibrium temperature, R is the universal gas constant, R = 8.314. $P_{2\text{H}_2\text{S},i}$ and $P_{3\text{H}_2\text{S},i}$ are the partial pressure of H_2S in

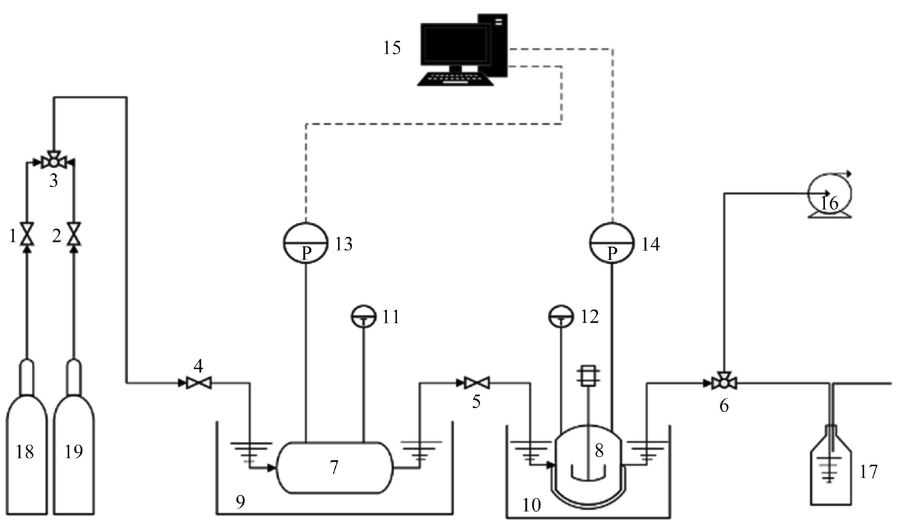

Fig. 1. The experiment flowchart of absorption (1–6: valve; 7: buffer tank; 8: equilibrium kettle; 9,10: water bath; 11,12: thermocouple; 13,14: pressure gauge; 15: computer; 16: vacuum pump; 17: absorption bottle; 18: nitrogen cylinder; 19: hydrogen sulfide cylinder).

the buffer tank before and after filling H_2S from the buffer tank to the phase equilibrium kettle in the *i*-th experiment. $P_{H_2S,i}$ is the equilibrium partial pressure of H_2S in the equilibrium kettle in the *i*-th experiment. $Z_{2,i}$, $Z_{3,i}$ and $Z_{H_2S,i}$ are the compression factors corresponding to $P_{2H_2S,i}$, $P_{3H_2S,i}$, and $P_{H_2S,i}$, respectively. These compression factors can be obtained by the PR thermodynamic method in Aspen Plus software (AspenONE® for Universities, Aspen Technology, Inc., Bedford, MA, USA).

$P_{2H_2S,i}$, $P_{3H_2S,i}$, and $P_{H_2S,i}$ are calculated by Eq. (7), Eq. (8), and Eq. (9).

$$P_{2H_2S,i} = P_{2,i} - P_1 \tag{7}$$

$$P_{3H_2S,i} = P_{3,i} - P_1 \tag{8}$$

$$P_{H_2S,i} = P_{4,i} - P_1 - P_L \tag{9}$$

where, $P_{2,i}$, $P_{3,i}$ are the pressure of the buffer tank before and after injecting H_2S to the phase equilibrium kettle in the *i*-th experiment. $P_{4,i}$ is the equilibrium pressure of the equilibrium kettle in the *i*-th experiment. P_1 is the pressure after the apparatus is vacuumized. P_L is the partial pressure of the solvent. The vapor pressure of the ionic liquid in this work is low, so $P_L = 0$. For solvents with high saturated vapor pressure, P_L cannot be ignored.

The solution volume V_L can be obtained from Eq. (10).

$$V_L = \frac{w_{Fe-IL}}{\rho_{Fe-IL}} \tag{10}$$

where $w_{Fe\text{-}IL}$ is the mass of the ionic liquid. $\rho_{Fe\text{-}IL}$ is the density of the ionic liquid. The experimental absorption pressure is low, and the density of ionic liquid with dissolved H_2S is approximately equal to that of pure ionic liquid.

3. Models

3.1. Density and viscosity models

Temperature variation of the density empirical correlation Eq. (11) [33] was used to fit the experimental data.

$$\rho = A + BT \tag{11}$$

where ρ ($g\cdot cm^{-3}$) is density, T (K) is temperature. A and B are fitting parameters, which are obtained by fitting the equation with experimental data through least square regression.

VFT empirical Eq. (12) [34] was used to fit the experimental viscosity data.

$$\eta = Ae^{B/(T-T_0)} \tag{12}$$

where η (mPa·s) is viscosity, T(K) is temperature, A, B and T_0 are parameters of the equation, which are obtained by fitting the experimental data.

Coefficient of determination (R^2), average relative error (ARD), and maximum relative error (MRD) are used to characterize the degree of fitting between the calculated value and the experimental data. These parameters are defined in the Supplementary Material.

3.2. Solubility model

Krichevsky-Kasarnovsky equation [35] and Henry's law [36] can be used to model the solubility of hydrogen sulfide in ionic liquid by physical absorption. The redox reaction of *r*$FeCl_3$/[A336]Cl occurred during the absorption of H_2S. Thus, chemical absorption should also be taken into account. Huang *et al.* [37] modeled the solubility of H_2S in 1-alkyl-3-methylimidazolium carboxylates ionic liquids using the reaction equilibrium thermodynamic model (RETM). Henry's constant and chemical reaction equilibrium constant could be estimated by the RETM fitting. Henry's constant characterized the physical solubility. The chemical reaction equilibrium constant characterized the chemical absorption. Wei *et al.* [38] applied the RETM to the mercapto carboxylic anions functionalized ionic liquid ([P4444][MSA]). Impressively, it was found that mercapto carboxylic anions captured H_2S through 1:1 and 2:1 mole ratio manner. Zhang *et al.* [39] used the RETM to fit the gas–liquid equilibrium data of H_2S in azole-based protic ionic liquid ([DBNH][1,2,4-triaz]). Furthermore, the enthalpy change of absorption was calculated according to the reaction equilibrium constant. Different ionic liquids and H_2S were combined in different ways, which resulted in various expressions of the RETM. In this work, the corresponding RETM was established by analyzing the process of *r*$FeCl_3$/[A336]Cl absorbing H_2S.

r$FeCl_3$/[A336]Cl has Bronsted acidic (Fig. S1 in the Supplementary Material), so the absorbed hydrogen sulfide mainly exists in the form of H_2S molecules. The physical absorption is presented as the following Eq. (13), which means that H_2S enters and dissolves in the ionic liquid from the gas phase.

$$H_2S_{(g)} \rightleftharpoons H_2S_{(l)} \tag{13}$$

where, subscripts *g*, and *l* denote gas and liquid phase, respectively.

According to the experimental results of H_2S absorption by [bmim]$FeCl_4$ ionic liquid reported by Wang *et al.* [40], ferric iron still exists at the absorption equilibrium. Therefore, the chemical reaction between *r*$FeCl_3$/[A336]Cl and H_2S can be considered reversible. According to the literature [22,30], the chemical absorption of H_2S in *r*$FeCl_3$/[A336]Cl is expressed by Eq. (14).

$$H_2S_{(l)} + 2Fe(III)\text{-}IL_{(l)} \rightleftharpoons S_{(s)} + 2HFe(II)\text{-}IL_{(l)} \tag{14}$$

In Eq. (14), subscript *s* denotes solid phases. *r*$FeCl_3$/[A336]Cl is considered a virtual molecule in the form of Fe(III)-IL. Reduced *r*$FeCl_3$/[A336]Cl is expressed as Fe(II)-IL. The Fe(II)-IL has similar properties to Fe(III)-IL, so the mixture of *r*$FeCl_3$/[A336]Cl + H_2S can be regarded as an approximate binary solution.

Based on the above assumption, Henry's equation of H_2S in *r* $FeCl_3$/[A336]Cl is expressed by the Eq. (15). Since the equilibrium pressure does not exceed 200 kPa, the fugacity of H_2S is replaced by partial pressure in Henry's equation.

$$P_{H_2S} = H_{app} \cdot \gamma_{H_2S} \cdot \frac{m_{H_2S}}{m^0} \tag{15}$$

where, P_{H_2S} (kPa) is the equilibrium partial pressure of H_2S. The vapor pressure of the ionic liquid is low. Thus, the gas phase in the equilibrium kettle can be considered as pure H_2S without solvent. m_{H_2S} (mol H_2S/kg IL, $mol\cdot kg^{-1}$) is the molality of the physically dissolved H_2S in liquid phase. m^0 (1 mol H_2S/kg IL, $mol\cdot kg^{-1}$) is the standard molality. γ_{H_2S} is the activity coefficient of H_2S in the liquid phase. H_{app} (kPa) is an apparent Henry's constant based on the assumption of a binary system.

The chemical absorption equilibrium of H_2S in ionic liquid is expressed in Eq. (14). The equilibrium constant K_{app} is given by Eq. (16).

$$K_{app} = \frac{\left(\gamma_{HFe(II)-IL}\frac{m_{HFe(II)-IL}}{m^0}\right)^2}{\left(\gamma_{Fe(III)-IL}\frac{m_{Fe(III)-IL}}{m^0}\right)^2 \gamma_{H_2S}\frac{m_{H_2S}}{m^0}} \tag{16}$$

where $m_{HFe(II)\text{-}IL}$ and $m_{Fe(III)\text{-}IL}$ are the molality of reacted and unreacted ionic liquids, respectively. $\gamma_{HFe(II)\text{-}IL}$ and $\gamma_{Fe(III)\text{-}IL}$ are the activity coefficients corresponding to $m_{HFe(II)\text{-}IL}$ and $m_{Fe(III)\text{-}IL}$, respectively. It should be pointed out that *r*$FeCl_3$/[A336]Cl is composed of $FeCl_4^-$, [A336]Cl^- and Cl^- ions. That is to say, the mixture of *r*$FeCl_3$/[A336]Cl + H_2S is a multicomponent solution. Therefore, K_{app} is also an apparent property.

The mass balance of H_2S and ionic liquids are expressed by Eq. (17) and Eq. (18), respectively.

$$m_t = m_{H_2S} + m_{H_2S,r} \tag{17}$$

$$m_{IL0} = m_{HFe(II)-IL} + m_{Fe(III)-IL} \tag{18}$$

where, m_t (mol H_2S/kg IL, mol·kg^{-1}) is the total solubility of H_2S. $m_{H_2S,r}$ (mol H_2S/kg IL, mol·kg^{-1}) is the molality of reacted H_2S. $m_{Fe(II)-IL}$ (mol/kg IL, mol·kg^{-1}) and $m_{HFe(II)-IL}$ (mol/kg IL, mol·kg^{-1}) are the molality of unreacted ionic liquid and reacted ionic liquid, respectively. According to Eq. (14), $m_{H_2S,r}$=1/2 $m_{HFe(II)-IL}$. m_{IL0} is the initial concentration of the ionic liquid based on mass, which can be calculated from Eq. (19).

$$m_{IL0} = \frac{1}{M_{IL0}} \tag{19}$$

where M_{IL0} (kg·mol^{-1}) is the molar mass of Fe(III)-IL. The molar mass of iron-based ionic liquids with different ratios r is shown in Table 2.

Under the experimental conditions, Fe(II)-IL has a similar structure and properties to Fe(III)-IL, so the liquid phase can be considered an ideal solution. The concentration of physically dissolved H_2S molecules in the solution is low. Thus, the activity coefficients γ_{H_2S}, $\gamma_{(Fe(III)-IL}$, and $\gamma_{HFe(II)-IL}$ are all 1. From Eqs. (15)–(19), the RETM for the absorption process of hydrogen sulfide by rFeCl$_3$/[A336]Cl is given by Eq. (20).

$$m_t = \frac{P_{H_2S}}{H_{app}} + \frac{m_{IL0}}{2}\left(\frac{\sqrt{K_{app}P_{H_2S}H_{app}} - K_{app}P_{H_2S}}{H_{app} - K_{app}P_{H_2S}}\right) \tag{20}$$

Taking P_{H_2S} and m_t as fitting data, Henry's constant (H_{app}) and the chemical reaction equilibrium constant (K_{app}) are obtained by ORIGIN software from the least squares fit of m_t with P_{H_2S}.

Table 2
The molecular weight of iron-based ionic liquids:

Molar ratio of $FeCl_3$ to [A336]Cl (r)	Molecular weight/kg·mol^{-1}
0.1	0.4203
0.2	0.4366
0.4	0.4690
0.6	0.5015
0.8	0.5339

4. Results and Discussion

4.1. Validation of the experimental method

The liquid gravity balance for density measurement was validated with pure water at atmospheric pressure and temperatures of 303 to 353 K. The results of the validation experiments were compared with data in the literature [41]. The results are shown in Table 3. In Table 3, RD is the relative deviation, which is defined in the Supplementary Material. It can be seen that the average relative error (ARD) is 0.0880%, and the maximum relative error (MRD) is 0.1017%. The digital viscometer for viscosity measurement was verified with glycerol at atmospheric pressure and temperatures of 323 to 365 K. The results of the validation experiments were compared with data in the literature [42]. The verification results are shown in Table 3. It can be found that ARD is 0.996% and MRD is 1.16%.

To verify the reliability of the solubility measurement device, the absorption of H_2S in pure water at a pressure range from 50 to 500 kPa was performed at 313.15 K, 323.15 K, and 333.15 K, respectively. To avoid solvent loss, the pressure after vacuumizing the device should be greater than the vapor pressure of water. The experimental steps are the same as those for determining the H_2S solubility in the ionic liquid. The data of the validation experiment are listed in Table 4, where P_{tot} is the total pressure of H_2S and H_2O.

Table 3
The density of water and viscosity of glycerol at (101.3±0.4) kPa

T/K	ρ/g·cm^{-3} Water			η/mPa·s Glycerol		
	This work	Literature	RD/%	This work	Literature	RD/%
303.15	0.9965	0.9956	0.0903			
313.15	0.9929	0.9922	0.0705			
323.15	0.9889	0.9880	0.0910			
323.88				145.80	147.40	−1.10
333.15	0.9842	0.9832	0.1016	85.42	84.71	0.83
343.15	0.9786	0.9778	0.0817			
343.80				49.25	49.83	−1.18
353.15	0.9727	0.9718	0.0925			
353.67				32.13	31.80	1.03
364.12				20.87	21.05	−0.86

Note: The measurement uncertainties u are $u(T)$ = 0.03 K, $u(\rho)$ = 0.0001 g·cm^{-3}, $u_r(\eta)$ = 0.01. T, equilibrium temperature; ρ, the density of liquid phase; η, the viscosity of the liquid phase; RD, relative deviation.

Table 4
H_2S solubility in pure water at T = 313.15 K, 323.15 K, and 333.15 K

T = 313.15 K		T = 323.15 K		T = 333.15 K	
P_{tot}/kPa	100·(x_t)	P_{tot}/kPa	100·(x_t)	P_{tot}/kPa	100·(x_t)
56.8	0.0766	53.2	0.0609	59.2	0.0585
107.2	0.1402	107.8	0.1206	128.3	0.1214
165.2	0.2133	165.4	0.1829	230.1	0.2146
214.6	0.2803	237.6	0.2615	304.9	0.2859
328.7	0.4311	310.6	0.3373	377.7	0.3540
390.0	0.5057	420.8	0.4538	430.2	0.3977

Note: Standard uncertainties u are $u(T)$ = 0.03 K, $u(P_{tot})$ = 0.6 kPa, $u(x_t)$ = 0.0150. T, equilibrium temperature; P_{tot}, the total pressure of H_2S and H_2O in the gas phase; x_t, the molar fraction of H_2S in the liquid phase; $u(x_t)$ is standard uncertainty of x_t.

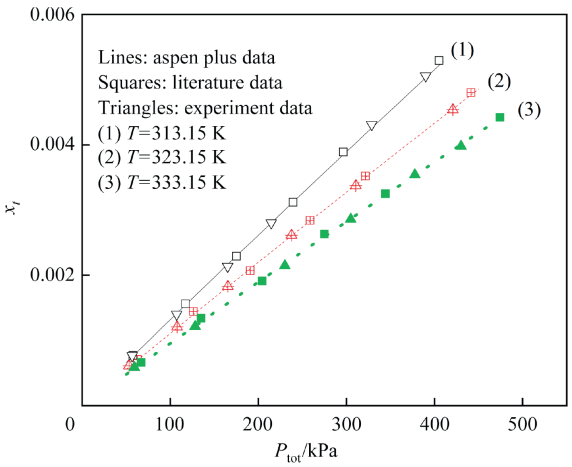

Fig. 2. Solubility of H_2S in pure water (50–500 kPa).

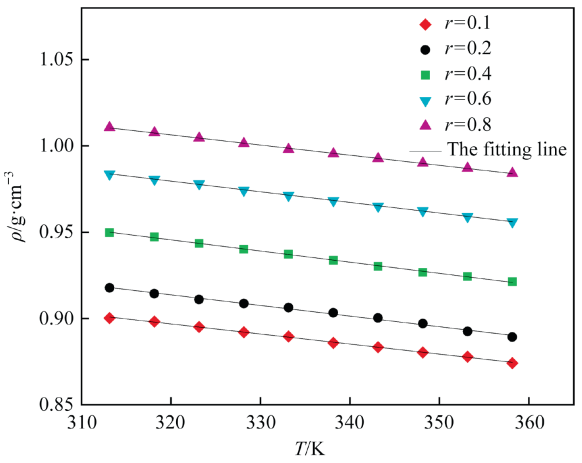

Fig. 3. Variation of density of rFeCl$_3$/[A336]Cl with the temperature at 101.13 kPa ± 0.4 kPa.

The results of the validation experiments were compared with calculations (the thermodynamic method is SRK) by Aspen Plus software (AspenONE® for Universities, Aspen Technology, Inc., Bedford, MA, USA) and data in the literature [43]. The results are shown in Fig. 2. The ARD% between the literature data and Aspen Plus data is 0.74%, and ARD% between the experimental data and Aspen Plus data is 0.62%. The results show that the experimental device is reliable.

4.2. Density

Under atmospheric pressure, the density data of rFeCl$_3$/[A336]Cl obtained through experiments within the temperature range of 313.15 to 358.15 K are shown in Table 5. Considering the effect of purity on the uncertainty of density measurement [44], the standard relative uncertainty of density of rFeCl$_3$/[A336]Cl is ±0.1%. The variation of experimental density with the temperature is shown in Fig. 3. It can be found that the density of rFeCl$_3$/[A336]Cl decreases with the decrease of iron content. The density of FeCl$_3$ is greater than that of [A336]Cl. As the iron content increases, that is, the molar ratio of FeCl$_3$ increases, and the density of rFeCl$_3$/[A336]Cl increases. Also it can be seen from Fig. 3 that the density of rFeCl$_3$/[A336]Cl decreases with the increase of temperature. With the increase of temperature, the molecular spacing increases, which leads to the decrease of the density of rFeCl$_3$/[A336]Cl. The density variation trend is consistent with the density law of FeCl$_3$/[Bmim]Cl ionic liquid studied by Li *et al.* [30]. The fitting results using Eq. (11) are shown in Table 6.

It can be seen from Table 6 that the prediction value has a good correlation with the experimental data of rFeCl$_3$/[A336]Cl. R^2 is greater than 0.99, ARD is not more than 0.07%, and MRD is not more than 0.12%. That means the empirical Eq. (11) can be used to predict the density of rFeCl$_3$/[A336]Cl.

Table 6
Parameter values of fitting Eq. (11) for density

r	A/g·cm^{-3}	B/g·cm^{-3}·K^{-1}	R^2	ARD/%	MRD/%
0.1	1.0833	-5.8279×10^{-4}	0.9986	0.0306	0.0566
0.2	1.1108	-6.1600×10^{-4}	0.9939	0.0694	0.1101
0.4	1.1523	-6.4618×10^{-4}	0.9987	0.0298	0.0658
0.6	1.1766	-6.1612×10^{-4}	0.9995	0.0165	0.0440
0.8	1.1943	-5.8775×10^{-4}	0.9990	0.0233	0.0561

4.3. Viscosity

At atmospheric pressure, the viscosity data of rFeCl$_3$/[A336]Cl measured within the temperature range of 313.15 to 358.15 K are shown in Table 7. The variation of viscosity with temperature and molar ratio (r) is shown in Fig. 4. It can be seen that the viscosity of rFeCl$_3$/[A336]Cl decreases with the increase of r, and the increase of temperature. The same conclusions were reported by Li *et al.* [30], who studied the effluence of iron content on the viscosity of FeCl$_3$/[C$_4$mim]Cl ionic liquid.

When the temperature is lower than 333.15 K, the viscosity changes significantly with temperature. For example, when the temperature increases from 313.15 K to 323.15 K, the viscosity of rFeCl$_3$/[A336]Cl with r = 0.1, 0.2, and 0.4 decreases by 50.9%, 45.2%, and 44.7%, respectively. When the temperature is higher than 333.15 K, the viscosity changes slowly with temperature.

Table 5
Density of rFeCl$_3$/[A336]Cl at T = 313.15 to 358.15 K at (101.3 ± 0.4) kPa

T/K	ρ/g·cm^{-3}				
	r = 0.1	r = 0.2	r = 0.4	r = 0.6	r = 0.8
313.15	0.9003	0.9178	0.9497	0.9836	1.0106
318.15	0.8982	0.9143	0.9472	0.9807	1.0076
323.15	0.8951	0.9110	0.9435	0.9780	1.0045
328.15	0.8921	0.9087	0.9401	0.9743	1.0013
333.15	0.8896	0.9063	0.9372	0.9713	0.9980
338.15	0.8859	0.9033	0.9337	0.9683	0.9953
343.15	0.8834	0.9003	0.9302	0.9650	0.9926
348.15	0.8803	0.8970	0.9267	0.9624	0.9900
353.15	0.8779	0.8925	0.9243	0.9590	0.9870
358.15	0.8742	0.8892	0.9213	0.9561	0.9840

Note: Standard uncertainties u are $u(T)$ = 0.03 K, $u_r(r)$ = 0.004, $u_r(\rho)$ = 0.001. T, equilibrium temperature; ρ, density of liquid phase; r, molar ratio of FeCl$_3$ to [A336]Cl.

Table 7
Viscosity of rFeCl$_3$/[A336]Cl at (101.3 ± 0.4) kPa

T/K	η/mPa·s				
	r = 0.1	r = 0.2	r = 0.4	r = 0.6	r = 0.8
313.15	1620.5	1027.0	599.1	273.4	156.7
318.15	1103.5	756.7	446.0	207.3	120.4
323.15	794.9	562.8	331.1	165.4	97.4
328.15	582.3	431.3	256.1	130.3	78.2
333.15	444.4	329.7	197.0	105.2	63.7
338.15	340.7	258.1	154.6	85.0	53.2
343.15	266.0	206.9	123.0	69.6	44.7
348.15	213.7	166.8	99.8	59.0	37.7
353.15	174.7	137.1	82.0	49.0	32.7
358.15	144.9	113.6	67.9	41.5	28.4

Note: Standard uncertainties u are $u(T)$ = 0.03 K, $u_r(r)$ = 0.004, $u_r(\eta)$ = 0.01. T, equilibrium temperature; η, viscosity of the liquid phase; r, molar ratio of $FeCl_3$ to [A336]Cl.

Table 8 shows that the VFT empirical equation has a good correlation with the temperature variation of the viscosity for rFeCl$_3$/[A336]Cl. R^2 is greater than 0.999. ARD is not more than 0.7%, and MRD is not more than 1.6%.

4.4. H_2S solubility

4.4.1. Measurement data

The gas–liquid equilibrium data of H_2S and rFeCl$_3$/[A336]Cl (r = 0.1–0.8) was measured at temperatures of 318.15 to 348.15 K and pressures of 0 to 150 kPa. The results are shown in Table 9 and plotted in Fig. 5. It can be seen that the total solubility of H_2S increases with pressure increasing and temperature decreasing. This is consistent with the solubility of most gases. When the pressure is lower than 50 kPa, the relationship between solubility and pressure is nonlinear, indicating that chemical absorption has a great influence. When the pressure is greater than 50 kPa, the solubility and pressure show an approximately linear

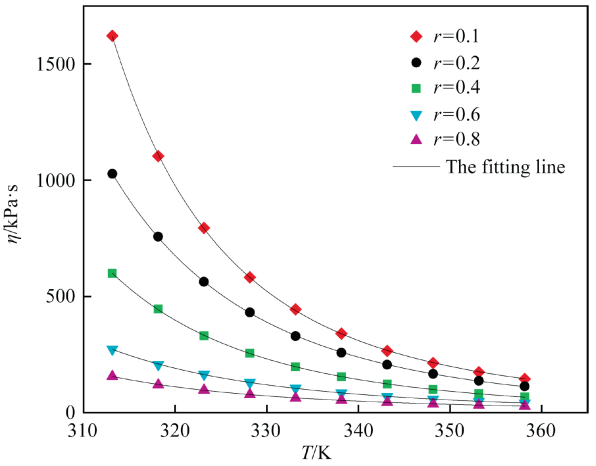

Fig. 4. Variation of viscosity of rFeCl$_3$/[A336]Cl with the temperature at 101.13 kPa ± 0.4 kPa.

Table 8
Parameter values of fitting Eq. (12) for viscosity

r	A/mPa·s	B/K	T_0/K	R^2	ARD/%	MRD/%
0.1	0.9828	693.1	219.5	0.9999	0.6157	1.1971
0.2	0.0682	1444.9	163.0	0.9999	0.5321	1.5422
0.4	0.0274	1599.0	153.2	0.9999	0.5898	1.5040
0.6	0.0806	1216.7	163.4	0.9998	0.5869	1.1225
0.8	0.3076	743.4	193.8	0.9998	0.3982	1.0188

Table 9
Experimental solubility data of H_2S in rFeCl$_3$/[A336]Cl: P_{H_2S}, partial pressure of H_2S in the gas phase; m_t, molality of H_2S in liquid phase; $u(m_t)$ is standard uncertainty of m_t; r, molar ratio of $FeCl_3$ to [A336]Cl

318.15 K		328.15 K		338.15 K		348.15 K	
P_{H_2S}/kPa	m_t/mol·kg^{-1}	P_{H_2S}/kPa	m_t/mol·kg^{-1}	P_{H_2S}/kPa	m_t/mol·kg^{-1}	P_{H_2S}/kPa	m_t/mol·kg^{-1}
r = 0.1							
10.0	0.1917	15.2	0.2345	10.5	0.1786	9.6	0.1435
25.5	0.3474	28.1	0.3348	30.8	0.3280	28.4	0.2561
39.5	0.4590	39.5	0.4147	43.0	0.4025	39.1	0.3084
77.6	0.7137	74.0	0.6314	73.3	0.5621	73.5	0.4455
123.7	1.0086	129.2	0.9338	127.1	0.8188	124.5	0.6311
r = 0.2							
8.8	0.2158	7.2	0.1873	6.0	0.1466	9.8	0.1712
22.6	0.3628	26.9	0.3526	29.4	0.3239	33.0	0.3047
39.0	0.4791	42.0	0.4439	44.8	0.4045	46.5	0.3607
71.3	0.6803	71.5	0.5951	78.1	0.5355	76.7	0.4649
127.2	0.9883	129.3	0.8417	126.3	0.6988	126.4	0.5990
r = 0.4							
10.6	0.2147	23.0	0.2881	7.0	0.1487	10.0	0.1551
32.1	0.3749	37.8	0.3746	24.9	0.2642	33.0	0.2705
51.6	0.4834	55.2	0.4491	40.4	0.3280	52.4	0.3319
71.9	0.5763	89.2	0.5663	79.3	0.4552	81.8	0.4073
129.4	0.8038	135.8	0.7159	137.3	0.5993	128.6	0.5039
r = 0.6							
5.4	0.1072	9.3	0.1182	12.7	0.1310	6.5	0.0803
16.5	0.1865	47.4	0.2749	35.2	0.2111	34.6	0.1836
30.7	0.2699	73.6	0.3517	62.3	0.2794	76.9	0.2692
68.5	0.4192	101.7	0.4194	106.1	0.3713	106.1	0.3133
132.2	0.6179	120.9	0.4605	126.4	0.4046	137.0	0.3543
r = 0.8							
7.7	0.0649	14.0	0.0876	13.5	0.0753	8.8	0.0519
15.1	0.1008	28.3	0.1310	26.0	0.1067	24.9	0.0881
29.2	0.1483	50.2	0.1821	42.4	0.1390	43.3	0.1200
76.9	0.2765	79.4	0.2403	80.9	0.1988	87.5	0.1734
145.7	0.4315	133.6	0.3295	125.8	0.2585	130.4	0.2139

Note: Standard uncertainties u are $u(T)$ = 0.03 K, $u_r(r)$ = 0.004, $u(P_{H_2S})$=0.6 kPa, $u(m_t)$ = 0.0159.

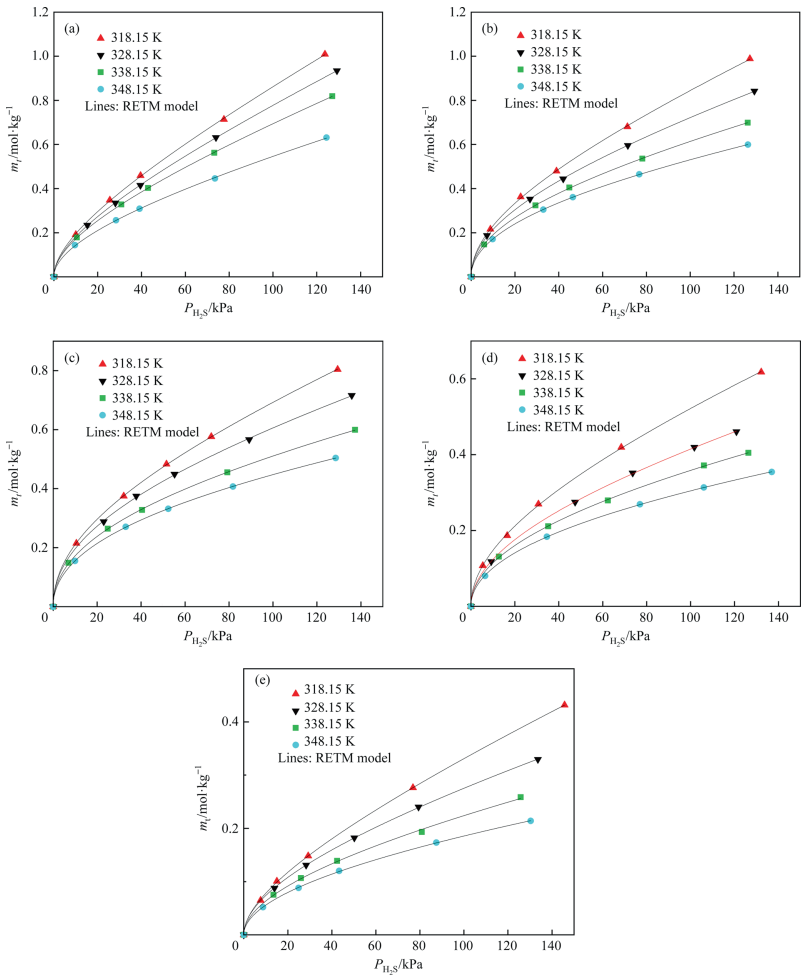

Fig. 5. Variation of H_2S partial pressure with molality of H_2S dissolved in rFeCl$_3$/[A336]Cl. (a) r = 0.1; (b) r = 0.2; (c) r = 0.4; (d) r = 0.6; (e) r = 0.8.

relationship, indicating that physical absorption has a great influence.

4.4.2. The RETM

The lines in Fig. 5 were calculated values using the RETM. Table 10 presents the fitting parameters of Henry's constant (H_{app}) and chemical reaction equilibrium constant (K_{app}). The ARD of the RETM for prediction is less than 1.3%, and the MRD is less than 3.4%. From Fig. 5 and Table 10, it can be seen that the RETM can predict the solubility of H_2S in rFeCl$_3$/[A336]Cl well.

Henry's constant can be used to characterize the physical solubility of H_2S in rFeCl$_3$/[A336]Cl. Fig. 6 shows the variation of Henry's constant (H_{app}) with the mole ratio (r) at different temperatures. It can be observed that Henry's constant increases with the increase of r. From Fig. 3 in Section 4.2, it can be observed that the larger r is, the greater the density is. That is to say, the free volume of the solution decreases with the increase of r, so fewer H_2S molecules can be accommodated [45,46]. Also can be seen from Fig. 6 that Henry's constant increases with the increase of temperature. Elevated temperature leads to the faster molecular motion of H_2S, which makes H_2S difficult to be immobilized in the liquid phase.

The chemical absorption of H_2S in rFeCl$_3$/[A336]Cl is characterized by the chemical reaction equilibrium constant. Fig. 7 shows the influence of the mole ratio (r) on the chemical reaction equilibrium constant (K_{app}). It can be seen that K_{app} increases with the increase of temperature, indicating that the forward chemical reaction that forms sulfur is endothermic. When r is less than 0.4, the concentration of $FeCl_4^-$ in rFeCl$_3$/[A336]Cl increases with the increase of r, and the oxidizing ability of ionic liquids becomes larger, and the chemical reaction equilibrium constant K_{app} increases.

However, in addition to oxidizing properties, r also affects the acidity of rFeCl$_3$/[A336]Cl. rFeCl$_3$/[A336]Cl is hydrophobic, so water cannot be used as a solvent for pH determination. According to the literature [47,48], ethanol can be used as the solvent to prepare 0.01 mol·L^{-1} ionic liquid-ethanol solution. pH values were measured directly by pH-meter (PHS-25, Shanghai Yueping Scientific Instrument Co., Ltd.) with a pH composite electrode (65-1C, Shanghai Yi Electrical Scientific Instrument Co., Ltd.). The measurement accuracy is ±0.01 pH. Before reading the value, the pH standard buffer solution was used to calibrate. The pH values of ionic liquid are shown in Table 11. It can be seen that with the increase of r, the pH of ionic liquid decreases, which means the acidity of the ionic liquid increases. This is due to the strongly acidic anions of $FeCl_4^-$ [21]. Therefore, with the increase of r, the acidity of rFeCl$_3$/[A336]Cl increases. The strong acidity is not conducive to the combination of rFeCl$_3$/[A336]Cl with acidic molecule H_2S, which leads to the decrease of K_{app}. This is consistent with conclusions on the effect of r on the acidity of imidazole-based Fe-ILs in the literature [49].

The joint action of the above two factors makes K_{app} increase first and then decrease with the increase of r, and the maximum value is reached when r = 0.4, as shown in Fig. 8.

Table 10
Henry's constant (H_{app}) and the chemical reaction equilibrium constant (K_{app}) were obtained from the RETM

	318.15 K	328.15 K	338.15 K	348.15 K
r = 0.1				
$H_{app} \pm u(H_{app})$/kPa	201.4 ± 2.8	235.0 ± 1.3	288.9 ± 2.1	427.8 ± 8.6
$K_{app} \pm u(K_{app})$	0.3945 ± 0.0227	0.4141 ± 0.0089	0.4929 ± 0.0119	0.5414 ± 0.0291
ARD/%	0.98	0.37	0.36	0.74
MRD/%	2.08	0.93	1.09	2.15
r = 0.2				
$H_{app} \pm u(H_{app})$/kPa	250.8 ± 3.7	349.8 ± 4.4	485.6 ± 6.6	682.8 ± 6.5
$K_{app} \pm u(K_{app})$	1.0176 ± 0.0490	1.3195 ± 0.0447	1.4840 ± 0.0458	1.7386 ± 0.0318
ARD/%	0.75	0.68	0.47	0.21
MRD/%	1.78	2.38	1.23	0.34
r = 0.4				
$H_{app} \pm u(H_{app})$/kPa	371.6 ± 3.3	515.3 ± 12.7	771.2 ± 16.1	1112.7 ± 13.1
$K_{app} \pm u(K_{app})$	1.6112 ± 0.0380	2.0397 ± 0.1144	2.3815 ± 0.0934	2.8360 ± 0.0540
ARD/%	0.42	0.74	0.65	0.20
MRD/%	1.03	1.20	1.97	0.41
r = 0.6				
$H_{app} \pm u(H_{app})$/kPa	482.4 ± 11.0	751.7 ± 15.3	1154.5 ± 40.9	1858.8 ± 61.4
$K_{app} \pm u(K_{app})$	1.0234 ± 0.0609	1.1648 ± 0.0519	1.6215 ± 0.1024	2.0954 ± 0.1073
ARD/%	1.00	0.47	0.68	0.58
MRD/%	2.65	0.99	1.68	2.05
r = 0.8				
$H_{app} \pm u(H_{app})$/kPa	629.8 ± 8.4	1013.0 ± 15.6	1559.4 ± 125.6	2580.1 ± 118.8
$K_{app} \pm u(K_{app})$	0.3196 ± 0.0135	0.5471 ± 0.0187	0.6592 ± 0.0972	0.8921 ± 0.0641
ARD/%	0.94	0.38	1.24	0.75
MRD/%	3.37	1.15	2.37	1.24

Note: r, the molar ratio of $FeCl_3$ to [A336]Cl; ARD, average relative error; MRD, maximum relative error.

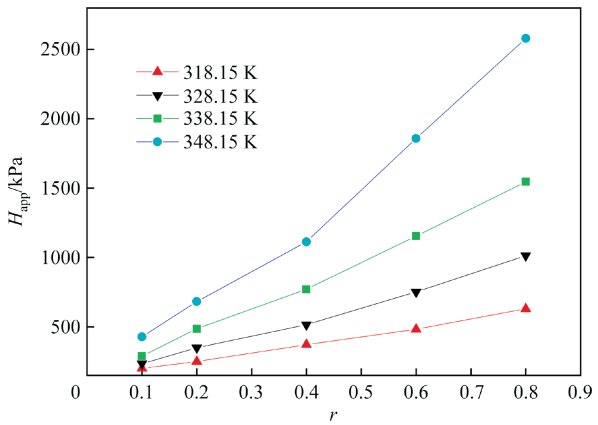

Fig. 6. The influence of r on H_{app}.

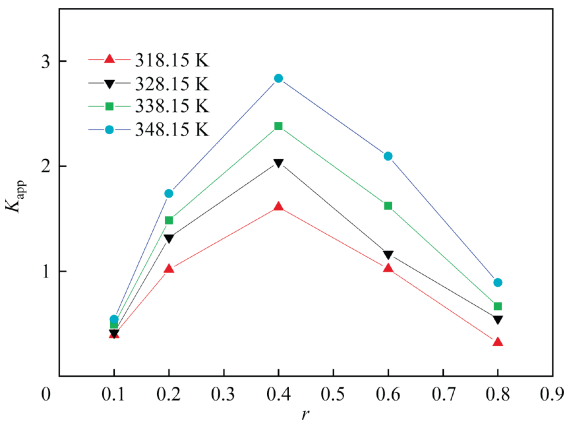

Fig. 7. The influence of r on K_{app}.

Table 11
The pH values of rFeCl$_3$/[A336]Cl ethanol solution at (298.15±0.03) K and (101.3±0.4) kPa

Molar ratio of $FeCl_3$ to [A336]Cl (r)	pH
0.1	2.95
0.2	2.60
0.4	2.40
0.6	2.15
0.8	1.90

Note: Standard uncertainty u is $u_r(r)$ = 0.004, $u(pH)$ = 0.01.

To understand the influence of the chemical reaction and the physical dissolution on the total solubility of H_2S in rFeCl$_3$/[A336]Cl, the amount of physical absorption and chemical absorption can be calculated according to Eq. (15) and Eq. (17), respectively. The chemical absorption isotherms and physical absorption isotherms of H_2S in rFeCl$_3$/[A336]Cl with r = 0.1 are plotted in Fig. 8. Chemical absorption isotherms and physical absorption isotherms with other r are given in the Supplementary Material. It can be seen from the figures that there is a linear relationship between the physical absorption of H_2S and the partial pressure of H_2S. When H_2S partial pressure is low, the chemical absorption curve is higher than the physical absorption curve, and the chemical absorption is dominant. When the partial pressure of H_2S reaches a certain value, the physical absorption curve is higher than the chemical absorption curve. Therefore, under high pressure, H_2S is mainly absorbed physically.

4.4.3. Effect of r on total solubility of H_2S

In addition to the influence of temperature and pressure on the solubility of H_2S in ionic liquid, the molar ratio (r) of $FeCl_3$ to [A336]Cl is also an important factor. At a certain temperature, the variation of the total solubility of H_2S with r is plotted in Fig. 9. It can be seen the total solubility of H_2S decreases with the increase of r in the whole pressure range (from 0 to 150 kPa)

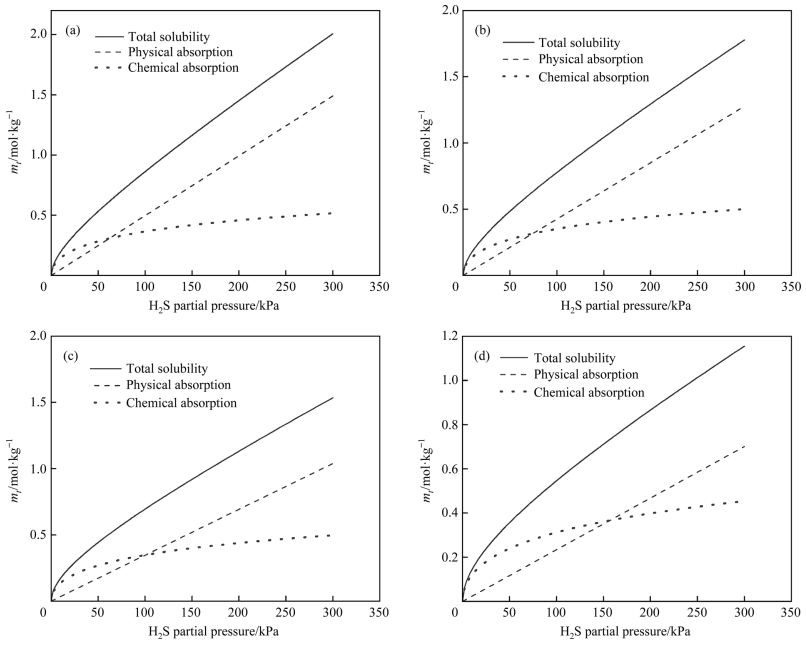

Fig. 8. Physical and chemical absorption curves of H_2S in 0.1$FeCl_3$/[A336]Cl. (a)T = 318.15 K; (b)T = 328.15 K; (c)T = 338.15 K; (d)T = 348.15 K.

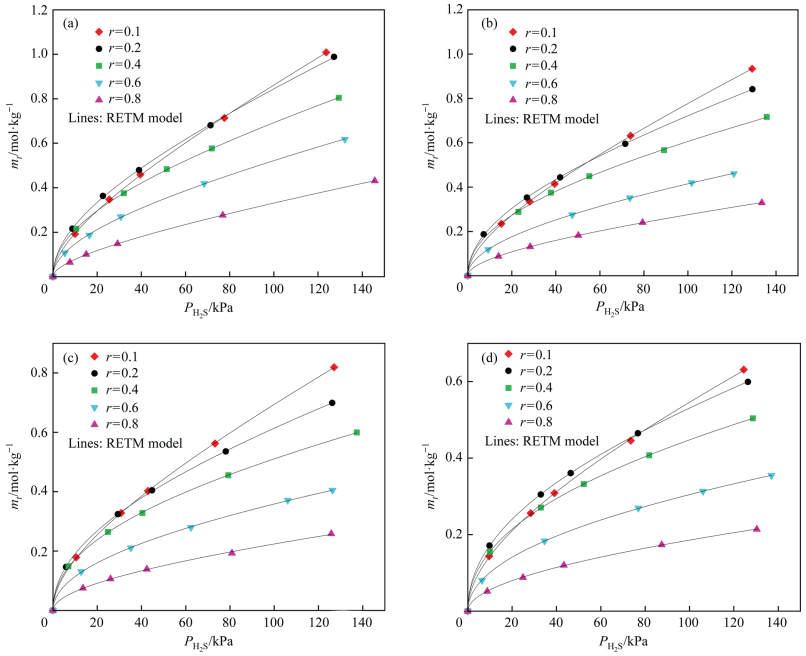

Fig. 9. The influence of r on the total solubility of H_2S. (a)T = 318.15 K; (b)T = 328.15 K; (c)T = 338.15 K; (d)T = 348.15 K.

when r ranges from 0.2 to 0.8. However, when r = 0.1 it presents a different pattern. With the increase of pressure, the total solubility of H_2S is first lower than that of r = 0.2, and then higher than that of r = 0.2. This is because the absorption of H_2S in 0.1$FeCl_3$/[A336]Cl has a smaller Henry's constant and chemical reaction equilibrium constant, which can be observed in Table 10.

Shah *et al.* [1] sorted out H_2S content in natural gas, biogas, syngas, and landfill gas. Natural gas had the highest H_2S content with a molar fraction of about 16%. Chemical absorption units generally operate at atmospheric pressure, so the maximum partial pressure of H_2S does not exceed 20 kPa. It can be seen from Fig. 9, when r = 0.2, $r$$FeCl_3$/[A336]Cl has the maximum total solubility under the H_2S partial pressure in the range of 0–20 kPa. This is because with the increase of r, for example, from 0.2 to 0.4, chemical reaction equilibrium constant increases. However, the corresponding Henry's constant increases at the same time. The increase of Henry's constant indicates that the amount of physically dissolved H_2S is reduced. Therefore, the amount of chemical absorption may not increase, which results in a reduction in total solubility.

4.5. Compared to other iron-based ionic liquids

Different anions and cations can form ionic liquids with different properties. Therefore, it will directly affect the solubility of H_2S in ionic liquids, Cheng *et al.* [31] measured the solubility of H_2S in iron-based ionic liquid $r$$FeCl_3$/[bmim]Cl ($r$ = 0.6, 0.8, 1.0, 1.2, 1.4) at

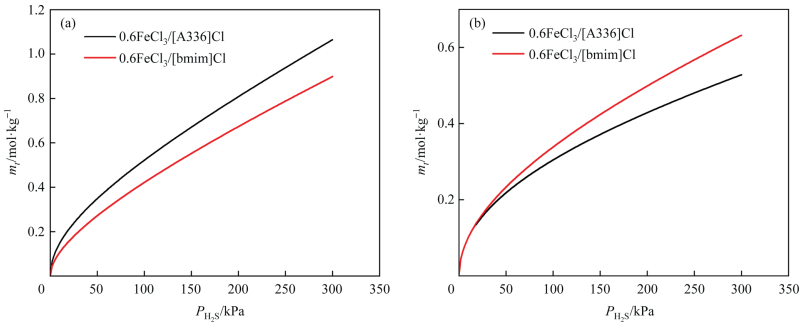

Fig. 10. Solubility of H_2S in two Fe-ILs at r = 0.6. (a) T = 318.15 K; (b) T = 348.15 K.

temperatures of 303.15 to 348.15 K and pressures of 100 to 1000 kPa. And corresponding Henry's constant and chemical reaction equilibrium constant were calculated. Therefore, the RETM was used to calculate the solubility of H_2S in rFeCl$_3$/[A336]Cl and rFeCl$_3$/[bmim]Cl at temperatures of 318.15 K and 348.15 K to compare the difference of H_2S absorption. For r = 0.6, the comparison of H_2S solubility are plotted in Fig. 10. The chemical reaction equilibrium constant and Henry's constant of two iron-based ionic liquids are shown in Figs. 11 and 12, respectively. For r = 0.8, results are given in the Supplementary Material.

It can be seen from Fig. 10 that the solubility of H_2S in rFeCl$_3$/[A336]Cl is greater than that of rFeCl$_3$/[bmim]Cl at the temperature of 318.15 K. This is due to that rFeCl$_3$/[A336]Cl has greater K_{app} and smaller H_{app}, which means rFeCl$_3$/[A336]Cl has greater reaction conversion and greater physical solubility. But at 348.15 K, Henry's constant and equilibrium constant of rFeCl$_3$/[A336]Cl are both larger than that of rFeCl$_3$/[bmim]Cl. Less physical solubility results in lower concentrations of reactants, which limits the amount of product from a chemical reaction. The difference of H_2S solubility of ionic liquids with temperature may be related to the different cationic structures of ionic liquids.

The raw material price of rFeCl$_3$/[A336]Cl is much lower than that of rFeCl$_3$/[bmim]Cl. In the actual wet desulphurization process, absorption is carried out under atmospheric pressure and normal temperature (lower than 318.15 K). Therefore, rFeCl$_3$/[A336]Cl has a better prospect of industrial application than rFeCl$_3$/[bmim]Cl.

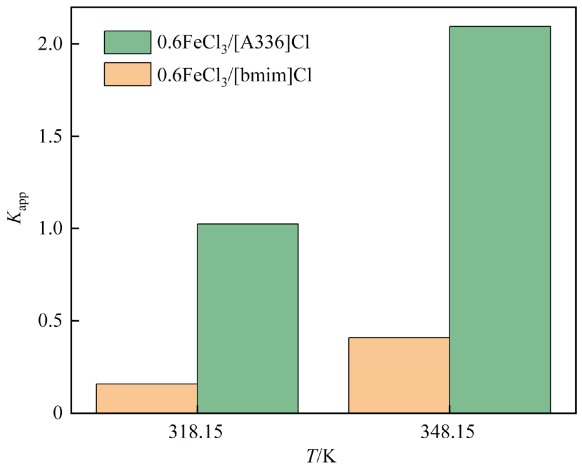

Fig. 11. The chemical reaction equilibrium constant (K_{app}) of two Fe-ILs with r = 0.6.

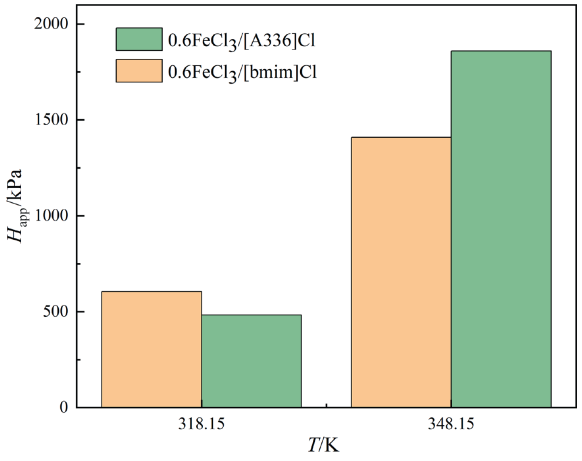

Fig. 12. Henry's constant (H_{app}) of two Fe-ILs with r = 0.6.

5. Conclusions

A new absorbent FeCl$_3$/[A336]Cl was proposed to absorb hydrogen sulfide from gas. The density and viscosity of rFeCl$_3$/[A336]Cl (r = 0.1–0.8) were measured at temperatures of 313.15 to 358.15 K and atmospheric pressure. Temperature-dependent empirical models correlate well with measurement data. The gas–liquid equilibrium data of H_2S in rFeCl$_3$/[A336]Cl was measured at temperatures from 318.15 to 348.15 K and pressures from 0 to 150 kPa. Henry's constant and chemical reaction equilibrium constant can be obtained by the RETM fitting, which can satisfactorily predict experimental results. For most gas desulphurization with H_2S partial pressure not more than 20 kPa, the maximum total solubility of H_2S in rFeCl$_3$/[A336]Cl is obtained at r = 0.2. Compared to rFeCl$_3$/[bmim]Cl ionic liquid, rFeCl$_3$/[A336]Cl has higher H_2S solubility and lower price, which makes rFeCl$_3$/[A336]Cl have a better potential for industrial application.

Declaration of Competing Interest

The authors declare that they have no known competing financial interests or personal relationships that could have appeared to influence the work reported in this paper.

Acknowledgements

Financial support from the National Natural Science Foundation of China (21775081) and Shandong Province Natural Science Foundation (ZR2020MB145) is gratefully acknowledged.

Supplementary Material

Supplementary data to this article can be found online at https://doi.org/10.1016/j.cjche.2022.11.012.

References

[1] M.S. Shah, M. Tsapatsis, J.I. Siepmann, Hydrogen sulfide capture: From absorption in polar liquids to oxide, zeolite, and metal-organic framework adsorbents and membranes, *Chem. Rev.* 117 (14) (2017) 9755–9803.

[2] A. Noyola, J.M. Morgan-Sagastume, J.E. López-Hernández, Treatment of biogas produced in anaerobic reactors for domestic wastewater: Odor control and energy/resource recovery, *Rev. Environ. Sci. Biotechnol.* 5 (1) (2006) 93–114.

[3] D.S. Gabbay, F.D. Roos, J. Perrone, Twenty-foot fall averts fatality from massive hydrogen sulfide exposure 1, *J. Emerg. Med.* 20 (2) (2001) 141–144.

[4] N. Abatzoglou, S. Boivin, A review of biogas purification processes, Biofuels, *Bioprod. Bioref.* 3 (1) (2009) 42–71.

[5] H.J. Son, J.H. Lee, H_2S removal with an immobilized cell hybrid reactor, *Process Biochem.* 40 (6) (2005) 2197–2203.

[6] M.O.H. Prc, Occupational exposure limits for hazardous factors in the workplace (GBZ 2.1-2007) Part 1: Chemical hazardous factors, China Standard Press, Beijing, 2007.

[7] H. Xu, D.D. Zhang, F.M. Wu, X.F. Wei, J. Zhang, Deep desulfurization of fuels with cobalt chloride-choline chloride/polyethylene glycol metal deep eutectic solvents, *Fuel* 225 (2018) 104–110.

[8] L. Sun, R. Smith, Rectisol wash process simulation and analysis, *J. Clean. Prod.* 39 (2013) 321–328.

[9] R.K. Srivastava, W. Jozewicz, Flue gas desulfurization: The state of the art, *J. Air Waste Manag. Assoc.* 51 (12) (2001) 1676–1688.

[10] G.T. Rochelle, Amine scrubbing for CO_2 capture, *Science* 325 (5948) (2009) 1652–1654.

[11] K.T. Li, M.Y. Huang, W.D. Cheng, Vanadium-based mixed-oxide catalysts for selective oxidation of hydrogen sulfide to sulfur, *Ind. Eng. Chem. Res.* 35 (2) (1996) 621–626.

[12] H. Zhang, X.M. Hu, Z.C. Liu, X.Q. Yang, X.J. Yang, Recovery of high purity elemental sulfur from coal syngas by liquid redox catalytic process using tannin extracts, *J. Clean. Prod.* 142 (2017) 3204–3211.

[13] A. Kazemi, M. Malayeri, A.G. Kharaji, A. Shariati, Feasibility study, simulation and economical evaluation of natural gas sweetening processes - Part 1: A case study on a low capacity plant in Iran, *J. Nat. Gas Sci. Eng.* 20 (2014) 16–22.

[14] J.C. Yue, C.L. Chu, W. Zhang, S.Q. Zheng, Influence of by-product salts and Na_2CO_3 contents on gas-liquid mass transfer process in wet desulfurization of water gas, *Clean Technol. Environ. Policy* 20 (6) (2018) 1367–1375.

[15] F. Liu, J. Yu, A.B. Qazi, L. Zhang, X. Liu, Metal-based ionic liquids in oxidative desulfurization: A critical review, *Environ. Sci. Technol.* 55 (3) (2021) 1419–1435.

[16] P.L.F. van den Bosch, O.C. van Beusekom, C.J.N. Buisman, A.J.H. Janssen, Sulfide oxidation at halo-alkaline conditions in a fed-batch bioreactor, *Biotechnol. Bioeng.* 97 (5) (2007) 1053–1063.

[17] R.L. Vekariya, A review of ionic liquids: Applications towards catalytic organic transformations, *J. Mol. Liq.* 227 (2017) 44–60.

[18] C. Verma, E.E. Ebenso, M.A. Quraishi, Ionic liquids as green and sustainable corrosion inhibitors for metals and alloys: An overview, *J. Mol. Liq.* 233 (2017) 403–414.

[19] B.E. Gurkan, T.R. Gohndrone, M.J. McCready, J.F. Brennecke, Reaction kinetics of CO_2 absorption in to phosphonium based anion-functionalized ionic liquids, *PCCP* 15 (20) (2013) 7796–7811.

[20] L.M. Galán Sánchez, G.W. Meindersma, A.B. de Haan, Kinetics of absorption of CO_2 in amino-functionalized ionic liquids, *Chem. Eng. J.* 166 (3) (2011) 1104–1115.

[21] J.H. Wang, R.R. Ding, Effect of water content on properties of homogeneous [bmim]Fe(III)Cl_4-H_2O mixtures and their application in oxidative absorption of H_2S, *Inorganics* 6 (1) (2018) 11.

[22] Y. He, J. Yu, L.B. Chen, Wet oxidation desulfurization of hydrogen sulfide with application of Fe-based ionic liquid, *CIESC J.* 61 (4) (2010) 963–968. (in Chinese)

[23] Z.H. Guo, T.T. Zhang, T.T. Liu, J. Du, B. Jia, S.J. Gao, J. Yu, Nonaqueous system of iron-based ionic liquid and DMF for the oxidation of hydrogen sulfide and regeneration by electrolysis, *Environ. Sci. Tech.* 49 (9) (2015) 5697–5703.

[24] Y.Q. Ma, R. Wang, H_2S absorption capacity and regeneration performance of amine Fe-based ionic liquids, *Chem. J. Chin. Univ.* 35 (4) (2014) 760–765.

[25] M. Li, J. Guan, J. Han, W.Z. Liang, K.K. Wang, E.H. Duan, B. Guo, Absorption and oxidation of H_2S in triethylamine hydrochloride · ferric chloride ionic liquids, *J. Mol. Liq.* 209 (2015) 58–61.

[26] D. Kogelnig, A. Stojanovic, F.v.d. Kammer, P. Terzieff, M. Galanski, F. Jirsa, R. Krachler, T. Hofmann, B.K. Keppler, Tetrachloroferrate containing ionic liquids: Magnetic- and aggregation behavior, *Inorg. Chem. Commun.* 13 (12) (2010) 1485–1488.

[27] J.H. Wang, X.P. Yu, M.S. Zhan, B. Xu, L. Zhu, Y.F. Wang, Oxidation absorption of H_2S by[bmim]OH and[A336][$FeCl_4$]mixed ionic liquids, *Nat. Gas Ind.* 38 (7) (2018) 100–107.

[28] D.F. Alves-Lima, C.F. Rodrigues, C.T. Pinheiro, L.M. Gando-Ferreira, M.J. Quina, A.G. Ferreira, Highly selective solvent extraction of Zn(II) and Cr(III) with trioctylmethylammonium chloride ionic liquid, *Can. J. Chem. Eng.* 100 (1) (2022) 131–142.

[29] T. Palden, M. Regadío, B. Onghena, K. Binnemans, Selective metal recovery from jarosite residue by leaching with acid-equilibrated ionic liquids and precipitation-stripping, *ACS Sustain. Chem. Eng.* 7 (4) (2019) 4239–4246.

[30] J.G. Li, Y.F. Hu, X.M. Peng, X.M. Zhang, Study on physicochemical properties of $FeCl_3$/[C_4mim][Cl]ionic liquids, *J. Chem. Thermodyn.* 97 (2016) 277–281.

[31] H.N. Cheng, N. Li, R. Zhang, N. Wang, Y.Y. Yang, Y. Teng, W.T. Jia, S.Q. Zheng, Measuring and modeling the solubility of hydrogen sulfide in r$FeCl_3$/[bmim]Cl, *Processes* 9 (4) (2021) 652.

[32] N. Wang, H.N. Cheng, Y. Wang, Y.Y. Yang, Y. Teng, C. Li, S.Q. Zheng, Measuring and modeling the solubility of carbon dioxide in protic ionic liquids, *J. Chem. Thermodyn.* 173 (2022) 106838.

[33] S.F. Shen, Y.N. Yang, Y. Wang, S.F. Ren, J.Z. Han, A.B. Chen, CO_2 absorption into aqueous potassium salts of lysine and proline: Density, viscosity and solubility of CO_2, *Fluid Phase Equilibria* 399 (2015) 40–49.

[34] L.S. Garca-Coln, D.C. Lf, P. Goldstein, Theoretical basis for the Vogel-Fulcher-Tammann equation, *Phys. Rev. B Condens. Matter* 40 (10) (1989) 7040–7044.

[35] T. Jia, S.S. Bi, J.T. Wu, Solubilities of carbon dioxide, oxygen, and nitrogen in aqueous ethylene glycol solution under low pressures, *Fluid Phase Equilibria* 485 (2019) 16–22.

[36] J. Safarov, C. Sperlich, A. Namazova, A. Aliyev, D. Tuma, A. Shahverdiyev, E. Hassel, Carbon dioxide solubility in 1-butyl-3-methylimidazolium tetrafluoroborate and 1-butyl-3-methylimidazolium tetrachloroferrate over an extended range of temperature and pressure, *Fluid Phase Equilibria* 467 (2018) 45–60.

[37] K. Huang, D.N. Cai, Y.L. Chen, Y.T. Wu, X.B. Hu, Z.B. Zhang, Thermodynamic validation of 1-alkyl-3-methylimidazolium carboxylates as task-specific ionic liquids for H_2S absorption, *AIChE J.* 59 (6) (2013) 2227–2235.

[38] L. Wei, Z.Y. Geng, Y.T. Liu, R.Z. Lu, Y.F. Xu, C.J. Liu, Y. Xu, Highly efficient and reversible H2S capture by mercapto carboxylic anion functionalized ionic liquids, *J. Mol. Liq.* 343 (2021) 116975.

[39] X.M. Zhang, W.J. Xiong, L.L. Peng, Y.T. Wu, X.B. Hu, Highly selective absorption separation of H_2S and CO_2 from CH_4 by novel azole-based protic ionic liquids, *AIChE J.* 66 (6) (2020) 16936.

[40] J.H. Wang, W.D. Zhang, Oxidative absorption of hydrogen sulfide by iron-containing ionic liquids, *Energy Fuels* 28 (9) (2014) 5930–5935.

[41] W.M. Haynes, D.R. Lide, T.J. Bruno, CRC Handbook of Chemistry and Physics, 95th Edition., Taylor & Francis Group, Oxford, 2014.

[42] A.G.M. Ferreira, A.P.V. Egas, I.M.A. Fonseca, A.C. Costa, D.C. Abreu, L.Q. Lobo, The viscosity of glycerol, *J. Chem. Thermodyn.* 113 (2017) 162–182.

[43] P. Fogg, C.L. Young, H. Clever, E.L. Boozer, W. Hayduk, Hydrogen sulfide, deuterium sulfide and hydrogen selenide, Pergamon Press, Oxford, 2013.

[44] R.D. Chirico, M. Frenkel, J.W. Magee, V. Diky, C.D. Muzny, A.F. Kazakov, K. Kroenlein, I. Abdulagatov, G.R. Hardin, W.E. Acree Jr, J.F. Brenneke, P.L. Brown, P.T. Cummings, T.W. de Loos, D.G. Friend, A.R.H. Goodwin, L.D. Hansen, W.M. Haynes, N. Koga, A. Mandelis, K.N. Marsh, P.M. Mathias, C. McCabe, J.P. O'Connell, A. Pádua, V. Rives, C. Schick, J.P.M. Trusler, S. Vyazovkin, R.D. Weir, J. T. Wu, Improvement of quality in publication of experimental thermophysical property data: Challenges, assessment tools, global implementation, and online support, *J. Chem. Eng. Data* 58 (10) (2013) 2699–2716.

[45] M.S. Shannon, J.M. Tedstone, S.P.O. Danielsen, M.S. Hindman, A.C. Irvin, J.E. Bara, Free volume as the basis of gas solubility and selectivity in imidazolium-based ionic liquids, *Ind. Eng. Chem. Res.* 51 (15) (2012) 5565–5576.

[46] X. Wang, S.J. Zeng, J.L. Wang, D.W. Shang, X.P. Zhang, J.D. Liu, Y.T. Zhang, Selective separation of hydrogen sulfide with pyridinium-based ionic liquids, *Ind. Eng. Chem. Res.* 57 (4) (2018) 1284–1293.

[47] E.H. Duan, B. Guo, M.M. Zhang, B.B. Yang, D.D. Zhang, pH measurements of caprolactam tetrabutyl ammonium bromide ionic liquids in solvents, *J. Chem. Eng. Data* 55 (9) (2010) 3278–3281.

[48] E. Bogel-ÅLukasik, U. DomaÅnska, pH measurements of 1-alkyl-3-methylimidazolium chloride in alcohols, *Green Chem.* 6 (6) (2004) 299–303.

[49] A.H. Jalili, A. Mehdizadeh, M. Shokouhi, A.N. Ahmadi, M. Hosseini-Jenab, F. Fateminassab, Solubility and diffusion of CO_2 and H_2S in the ionic liquid 1-ethyl-3-methylimidazolium ethylsulfate, *J. Chem. Thermodyn.* 42 (10) (2010) 1298–1303.